Simulation of Gain and Timing Resolution in Saturated Pores

Valentin Ivanov,[a*] Zeke Insepov,[b] Sergey Antipov[b]

[a]*Muons, Inc.,552 N. Batavia Ave., Batavia, IL 60610, USA*

[b]*Argonne National Laboratory, 9700 S. Cass Avenue, Argonne, IL 60439, USA*

Elsevier use only: Received date here; revised date here; accepted date here

Abstract

Micro-channel plate (MCP) amplifiers are commonly used in detectors of fast time signals with a picosecond resolution. The main parameters of the MCP amplifier, such as the gain factor and time resolution are strongly dependent on the work regime of the device. The saturation effects occur with a high-level input signal. In our paper these effects are studied numerically for large-area fast photo-detectors. It is shown that the saturation effect for short pulses can be reduced by introducing a thin, resistive layer between the bulk material and the emissive coating. A set of 2D and 3D numerical tools (MCP simulator, Monte Carlo simulator) was developed to simulate photo, secondary emission, fringe fields, and saturation phenomena in MCP amplifiers. The gain and time resolution dependencies on the pore size and voltage were studied numerically. The results are compared with the simulations of other authors and available experimental data.

PACS: 34.35.+a, 79.20.Hx, 02.70.Uu, 42.79.Pw

Keywords: micro channel plate; secondary emission; saturation; gain; timing resolution;

1. Introduction

Many measurements in particle and accelerator physics are limited by the time resolution with which individual particles can be detected. These measurements include particle identification by time of flight in major experiments such as CDF at Fermilab and Atlas and CMS at the Large Hadron Collider, as well as measurement of longitudinal variables in accelerator physics experiments.

A large-area photo-detector consists of the photo-cathode accepting photons from a Cherenkov counter, a microchannel plate (MCP), a segmented anode and accelerating gaps between them (Fig.1). The MCP produces cascades of secondary electrons to be detected by the anode circuit.

Figure 1. MCP photo detector.

* Corresponding author. Tel.: +1-408-568-1483; e-mail: vivanov@fnal.gov.

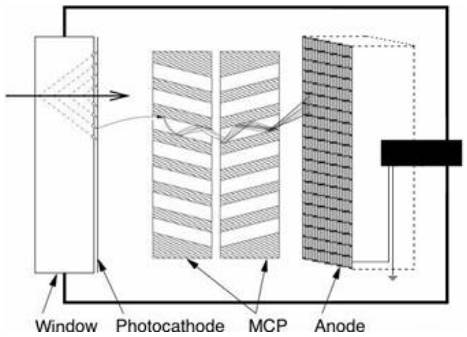

MCP amplifiers have been studied numerically by many authors [1]-[3].

2. Numerical model of saturation effect

As it was shown by A. Guest [1], the longitudinal current distribution in the pore has an exponential dependence. This means that a huge number of secondary electrons are extracted from the end of the pore for short input pulse and high gain, and a positive charge is induced on the pore surface thereby suppressing further secondary emission. The current from an external source cannot compensate for the induced charge immediately because of the finite resistance of the secondary emitter material. The saturation effect can be mitigated by two approaches. The first is to make a double-layer cover on the pore surface: a high-conductivity layer below and a high-emission layer on top. The second approach can be realized in a MCP chevron pair or Z-stack by varying the interpolate gap. Here the secondary electron beam from the first plate is redistributed to the neighbor pores of the second plate. This approach reduces the current in an individual channel, and reduces the saturation affect. We studied both these approached numerically.

Different models of the saturation effect in an MCP have been suggested in publications [4]-[6]. All of them include some coefficients to fit the gain vs. voltage dependence to the experimental data. A. Berkin and V. Vasil'ev give an analytical solution for the pulse [7] and DC [8] work regimes, which include the easily measured parameters only for the electric field

$$E_z(z,t) = E_{0z} h_E(z,t), \qquad (1)$$

and gain

$$M(z,t) = M_0 \frac{h_E(z,t)}{1 - [h_E(z,t_p) - 1]\exp\left(\frac{t_p - T}{\tau}\right)}. \qquad (2)$$

The shape function is given by the following formulas

$$h_E(z,t) = \frac{\ln(M_0)}{[\ln(M_0) - \ln(1 + C(t)) - \ln(1 + C(t)M_0)][1 + C(t)e^{\alpha z}]},$$

$$c(t) = \frac{I_0}{I_R}\left(1 - e^{-t/\tau}\right). \qquad (3)$$

Here E_{0z}, M_0 are the electric field and gain for the non saturated mode; T, t_p are the pulse period and pulse length; τ is a charge relaxation time (CRT); I_0, I_R are the input current and resistance current; α is the increment of the emission current in non-saturated pore $I(z)=I_0 \exp(\alpha z)$, z *is the* axial coordinate; t is the time.

Figures 2-3 show the results of our simulations for 20 μm pores of 1.2 mm length. One can see that the saturation effects are negligible for I_0 < 1.e-15 A.

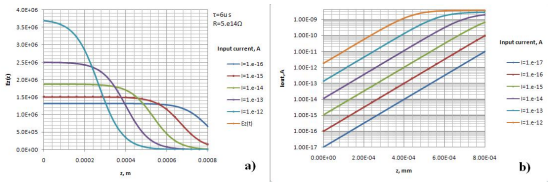

Figure 2. (a) Field distribution in the channel for different input current; (b) Output current distribution vs. input currents.

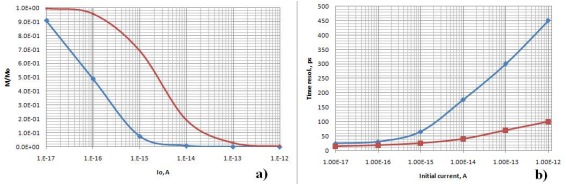

Figure 3. (a) Gain vs. input current for τ=1 msec (blue) and τ=1usec (red); (b) Timing resolution vs. input current.

3. Fringe field simulation in 3D

We have simulated the electric field inside the pores of chevron-type MCPs using the multi physics COMSOL software and verified this study by an analytical solution. The simulations show that in a highly-conductive environment, the electric field in the pore is directed axially inside the pore, having a gradual turn from the value in the resistive layer near the surface. In a simulation we assume that the relaxation time ε/σ is small for a thin resistive layer comprising a mixture 30% Al_2O_3 and 70% ZnO.

Fig. 4 shows the streamlines of electric field in 1 and 7 pores with bias angle of 8˚.

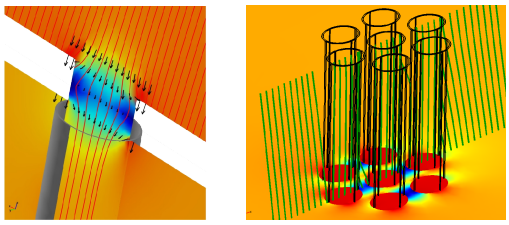

Figure 4. Streamlines of electric field in the pores.

Figure 5 demonstrates the edge effect at the end of pore.

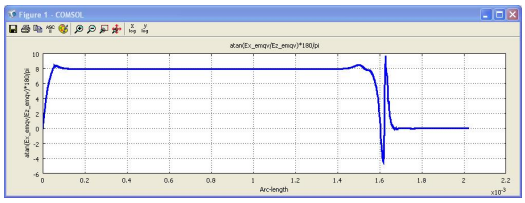

Figure 5. Edge effect for the electric field.

4. Charge relaxation time computation

ZnO/Al_2O_3 alloy films were prepared by using atomic layer deposition (ALD) techniques. By adjusting the ALD pulse sequence, the ZnO/Al_2O_3 alloy film composition was varied from 0% to 100% ZnO [10]. Figure 6 shows the resistivity of ZnO/Al_2O_3 alloy films used in this work. The material constants and physical properties of these alloy films, such as surface roughness, resistivity, dielectric constants, and film thickness were selected so that these materials could be used as resistive and emissive layers in large-area photo detecting MCPs, as compared with conventional glass substrates. Charge relaxation and gain depletion mechanisms, effects of a strong electric field, and geometry parameters of the coating for large-area, fast photo detectors were analyzed and discussed in Ref. [11].

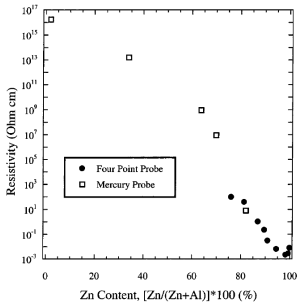

Fig. 6. Measured resistivity of ZnO/Al_2O_3 alloy films.

A new ambipolar solid state plasma drift-diffusion model of the charge relaxation in such materials as ZnO/ Al_2O_3 in various combination of the content was proposed that included generation of electrons and holes via impact ionization due to acceleration in a strong electric field [12]. Some of the equations of this model are given below [13-16]:

$$\vec{J}_e = eD_e\nabla N_e + e\mu_e N_e\vec{E},$$

$$\vec{J}_h = -eD_h\nabla N_h + e\mu_h N_h\vec{E},$$

$$div\,\vec{E} = \rho/\varepsilon\varepsilon_0, \rho = N_h - N_e,$$

$$\frac{\partial N_e}{\partial t} = \frac{1}{q}\nabla J_e = D_e\Delta N_e + eN_e\mu_e/\varepsilon\varepsilon_0(N_h - N_e) + G_{ii},$$

$$\frac{\partial N_h}{\partial t} = -\frac{1}{q}\nabla J_h = D_h\Delta N_h - eN_h\mu_h/\varepsilon\varepsilon_0(N_h - N_e),$$

$$\mu_{e,h} = \sigma_{e,h}/eN_{e,h},\ D_{e,h} = \mu_{e,h}k_BT/e.$$

Here e is the elemental charge amount ($e > 0$), $D_{e,h}$ are the diffusion coefficients, and $\mu_{e,h}$ are the mobility of electrons and holes at temperature T created by electron impacts and ionization in the space charge field, G_{ii}. The Einstein relationship between the diffusion coefficients and the mobility allows use of the electric-field-dependent diffusion coefficients; $N_{e,h}$ are the corresponding carrier densities; and $J_{e,h}$ are the fluxes of carriers.

The following conductivity of *AZO* film with 20% Al was used: $\mu = 10^7$ (Ω cm). The diffusion coefficients of amorphous alumina are unknown. Therefore, we used the diffusion coefficients of alumina via alumina carrier mobility that are given for some limited mixture content in Ref. [17]. Assuming linear dependence between conductivity and mobility, the mobility of a mixture Al_2O_3+ZnO was extrapolated from low to high Al content.

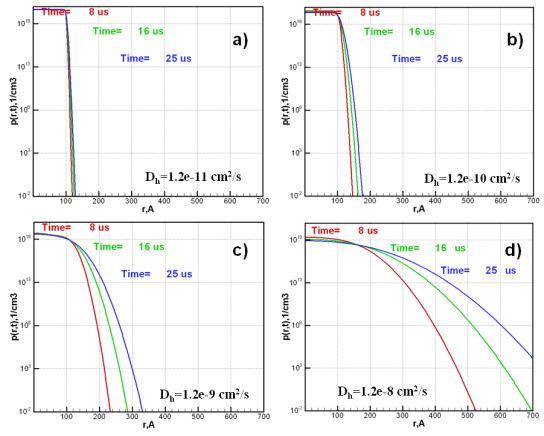

Fig. 7. Results of our calculation with the drift-diffusion model in spherical geometry, with the diffusion coefficients shown in the plots: (a) 1.2×10^{-11}, (b) 1.2×10^{-10}, (c) 1.2×10^{-9}, and (d) 1.2×10^{-8} cm^2/s.

The calculated results (Figure 7) were compared with the results of a simple Maxwell relaxation time model and with the circuit charge relaxation model developed for the MCP device [18]. A pump-probe experiment is in principle capable of measuring the charge relaxation time, and to clearly demonstrate gain depletion [19].

5. Mitigation of saturation effect

Monte Carlo algorithm is commonly used in simulation of MCP amplifiers [9]. The effect of inter-plate gap variation was studied numerically with using full 3D Monte Carlo Simulator (MCS) code. Fig. 8 shows that most of the beam from the first plate is accepted by one pore of the second plate for a gap size of 15 μm. The same initial beam is redistributed for 7 pores of a hexagonal structure in a second MCP for a gap of 100 μm (Fig. 9), which is substantially reduces the saturation effect.

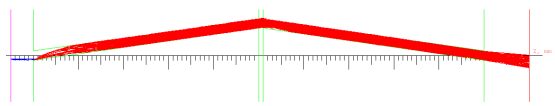

Figure 8. Small gap: gain M=1.2E6 for τ=1μs, and M=1.5E5 for τ=1ms. Blue – photo electrons; red – secondary electrons.

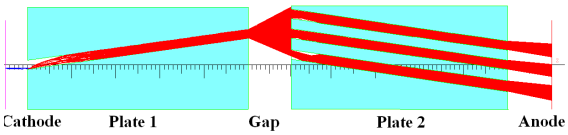

Figure 9. Large gap. Electrons distributed to 7 pores of the second plate. Gain M=3.4E6 for τ=1μs, and M=1.13E6 for τ=1ms.

References

[1] A. J. Guest, Acta Electron. 14, 1 (1971) 79-97
[2] A. M. Tutikov et al., Sov. J. Opt. Technol. 50, 7 (1991) 392-395
[3] A. S. Tremsin et al., Nucl. Inst. Meth. A379 (1996) 139-152
[4] P. M. Shikhalev, Nucl. Inst. Meth. A420 (1999) 202-212
[5] G. J. Price, G. W. Fraser, Nucl. Inst. Meth A474 (2001) 188-196
[6] G. W. Fraser et al., IEEE Trans. Nucl. Sci. NS-30, 1 (1983) 455-460
[7] A. B. Berkin, V. V. Vasil'ev, Zhurn. Techn. Fiziki, 78, 2 (2008) 127-129
[8] A. B. Berkin, V. V. Vasil'ev, Zhurn. Techn. Fiziki 78, 2 (2008) 130-133
[9] E. Gatti et al., IEEE Trans. Nucl. Sci. NS-30, 1 (1983) 461-467
[10] J. W. Elam et al., J. Electrochem. Soc. 150**,** 6 (2003) G339-G347
[11] A. K. Jonscher, Principles of semiconductor device operations, Wiley (1960).
[12] A. G. Chynoweth, J. Appl. Phys. 31 (1960) 1161-1165
[13] A. H. Marshak, Proc. IEEE 72 (1984) 148-164
[14] R. Van Overstraeten, Solid St. Electronics 13 (1970) 583-608
[15] L.M. Biberman, Proc. IEEE 59 (1972) 555-572
[16] Z. Insepov et al., Phys. Rev. A77 (2008) 062901
[17] F. Ruske et al., J. Appl. Phys. 107 (2010) 013708
[18] A. B. Berkin, V. V. Vasil'yev, Techn. Phys. Lett. 33 (2007) 664-666
[19] O. L. Landen et al., Proc. SPIE, 2002 (1993) 2-5